Int. J. Environ. Sci. Technol. (2017) 14:2093–2108
DOI 10.1007/s13762-017-1295-1

ORIGINAL PAPER

Facile synthesis of hexamine–silicotungstic acid hybrid and its photocatalytic activity toward degradation of dyes

S. Mohammadghasemi-Samani[1] · M. Taghdiri[1,2]

Received: 5 August 2016 / Revised: 7 January 2017 / Accepted: 21 February 2017 / Published online: 13 March 2017

Abstract A new organic hybrid of silicotungstic acid was prepared by means of an easily available, very cheap, and non-toxic amine via a facile precipitation method. Characterization of hybrid was carried out by elemental analyses, Fourier transform infrared spectroscopy, powder X-ray diffraction, thermogravimetric analysis, differential scanning calorimetry, and scanning electron microscopy. Dye adsorption and photocatalytic properties of the prepared water-insoluble hybrid were examined by studying the decolorization of model dyes such as methylene blue and methyl, orange and their mixture solutions under ultraviolet, visible, and sunlight irradiation. The effect of different factors containing the initial concentration, pH, catalyst dosage, H_2O_2 dosage, and salt adding was investigated on the decolorization of dyes. The results showed that the hybrid is a good heterogeneous photocatalyst in the degradation of methylene blue, methyl orange and their mixture and can be recovered and reused. The methylene blue is removed via combination of adsorption and photocatalytic degradation under ultraviolet, visible, and sunlight through direct oxidation by hybrid. The methyl orange is removed via ultraviolet and solar photocatalytic degradation through indirect oxidation by $^{\cdot}OH$ radicals. While the visible light is not able to degrade methyl orange solution alone in the presence of hybrid, it degrades the methyl orange mixed with methylene blue solution.

Keywords Decolorization · Methyl orange · Methylene blue · Photocatalyst · Polyoxometalate

Introduction

The most important contaminants of water are organic pollutants such as dyes, phenolics, and pharmaceuticals which cause many problems for the environment. Dyes are widely applied in the production of paints and textile, as an additive in plastic, paper, leather, cosmetics, and rubber industries, and so on (Hunger 2007). Discharge of wastewater of these industries creates serious threat for living organisms and human health due to toxicity and carcinogenicity (Deng et al. 2016a, b). Consequently, treatment of dye wastewaters with appropriate procedures is necessary before their discharge. Adsorption especially by activated carbon (AC) and AC composites is one of the most widely used and effective physical methods for removing dyes from wastewater (Afkhami et al. 2010; Fetterolf et al. 2003; Giri et al. 2011; Hu et al. 2014; Jiang et al. 2015; Li et al. 2015; Liu et al. 2012, 2015; Madrakian et al. 2011, 2012; Rajabi et al. 2015; Song et al. 2015; Yang et al. 2008, 2011; Zargar et al. 2009, 2011; Zhang and Kong 2011); however, these methods only transfer the pollutant from one phase to another (hence, the disposal of residues is still a problem). Advanced oxidation processes (AOPs) are widely used as a suitable method for wastewater treatments due to complete degradation of organics into carbon dioxide and water. Among various AOPs,

Editorial responsibility: Binbin Huang.

Electronic supplementary material The online version of this article (doi:10.1007/s13762-017-1295-1) contains supplementary material, which is available to authorized users.

✉ M. Taghdiri
mehditaghdiri@yahoo.com

[1] Department of Chemistry, Payame Noor University, Tehran 19395-3697, Iran

[2] Research Center of Environmental Chemistry, Payame Noor University, Ardakan, Yazd, Iran

heterogeneous photocatalysis has attracted much attention due to its low-cost, environmental friendliness and sustainability (García-López et al. 2016; Omwoma et al. 2015). Therefore, exploring some novel photocatalytic materials with high activities (especially under visible and sunlight irradiation) has drawn great attention (Deng et al. 2016a, b; Kwiatkowski et al. 2017; Pu et al. 2017). Recently, considerable attention has been focused on heteropoly acids including their anions (polyoxometalates or POMs) due to much superiority such as easy preparation, high reactivity, non-corrosive, non-toxicity, and outstanding stability. These compounds have been used as photocatalysts for the reductive destruction of dyes (Dolbecq et al. 2012). Nevertheless, although POMs display excellent photocatalytic effect, their high solubility in water and polar solvents causes difficulties in the separation and recycling from the reaction system (Wang and Yang 2010). Hence, developing efficient heterogeneous POM photocatalysts is needed. One of the approaches for the generation of POM-based heterogeneous catalysts is hybridization of POM species with organic compounds especially amines (Dolbecq et al. 2012; García-López et al. 2016; Omwoma et al. 2015).

One of the heteropolyacids is silicotungstic acid ($H_4SiW_{12}O_{40}$, STA) that has Keggin structure, i.e., it includes a heteroatom, as SiO_4 and the addenda atom W. A SiO_4, in the center, assembled with four peripheral $[W_3O_{13}]$ units that create 12 octahedra in total, whose centers are occupied by tungsten. Keggin $SiW_{12}O_{40}^{4-}$ can be obtained by a facile polycondensation reaction between the silicate and tungstate ions in an acidic aqueous medium. STA along with its hybrid materials are recently taken into account in some new important branches of science such as solar hydrogen production (Liu et al. 2016; Muradov and T-Raissi 2006), energy storage application (Hazra and Chatterjee 2013), photochromic materials (Gamelas et al. 2002; He and Yao 2006; Huang et al. 2006), solar cells (Kida et al. 2015; Ye et al. 2016), corrosion protection (Herrmann et al. 2014), and photodegradation of pollutants particularly dyes.

A facile precipitation method is presented to prepare a new organic hybrid of STA as heterogeneous photocatalyst. Hexamine or hexamethylenetetramine (HMT), an easily available compound produced by the reaction of ammonia with formaldehyde (Alamdari and Tabkhi 2004), is used for the preparation of hexamine–silicotungstate (HMT–STA) hybrid. HMT $(CH_2)_6N_4$, is an amine which possesses three fused rings in the chair conformation with a cage-like structure (Taghdiri et al. 2013). It is very cheap and non-toxic unlike other amines. The photocatalytic performance of water-insoluble hybrid was evaluated via photodegradation of methylene blue (MB), methyl orange (MO), and a mixture of MB and MO solutions under ultraviolet (UV), visible, and sunlight irradiation.

This research was carried out in Research Center of Environmental Chemistry, Payame Noor University of Ardakan, Yazd, Iran. The research began in September 2014 and completed in March 2015.

Materials and methods

Chemicals and reagents

STA (>99%) and H_2O_2 (aqueous solution, 35 wt%) were purchased from Merck. The HMT powder (99.5%) was supplied by Sina Chemical Industries Co. (Shiraz, Iran). Other reagents were purchased from commercial sources and used without further purification.

Apparatus

An analytical balance model Sartorius MCBA 100 with precision of ±0.0001 g was used for weighing of materials. Stirring of solutions was performed using a Labinco magnetic stirrer model L-81. For pH measurements, a Metrohm type 691 pH meter was used. A GBC UV–Vis spectrophotometer model Cintra 6 or Jenway 6010 spectrophotometer was used for spectrophotometric measurements. PerkinElmer 2400 CHN elemental analyzer was used for C, H, and N elemental analyses. A Shimadzu 8400 s FTIR spectrometer was applied for obtaining IR spectra using KBr pellets. A scanning electron microscope SEM PHENOM was used for the morphology characterization of the hybrid. The sample was as powder. A Bruker D8 advance X-ray diffractometer containing Cu target was used for obtaining X-ray diffraction patterns at room temperature. A Rheometric Scientific STA 1500 thermal analyzer was used for thermogravimetric analysis (TGA) and differential scanning calorimetry (DSC) under air atmosphere.

Preparation of photocatalyst

HMT–STA hybrid was prepared as follows: 10 mL aqueous solution of HMT (1.0% w/w) was added to 10 mL aqueous solution of STA (5% w/w). A milky suspension solution was produced immediately. The mixture was stirred at 500 rpm by a magnetic agitator at ambient temperature for 3 h. Then, a white precipitate resulted. The suspension was separated and the collected solid was washed with distilled water and then dried at 100 °C.

Photocatalytic activity for degradation of dyes

Photocatalytic with sunlight

Solar photocatalytic experiments were performed in the Pyrex glass vessel containing 20 mL MB or MO (5–20 mg/L) and 10–20 mg of HMT–STA. The solutions were irradiated under direct solar radiation in consecutive sunny days in September 2014 between 11 am and 3 pm (GPS coordinates: N = 32°29′, E = 53°59′). The solar radiation intensity in Yazd Province is about 800 W/m^2 in summer (Baghernejad and Yaghoubi 2010). The solutions were not stirred during solar irradiation.

Photocatalytic with UV and visible sources

Photocatalytic degradation process was also carried out under UV and visible light irradiation. A 250-W high-pressure mercury lamp and a metal halide lamp (500 W, Philips) were used as UV and visible light sources, respectively. The 50 mL dye solution with 25–50 mg of HMT–STA catalyst was stirred continuously in a 200-mL water-cooled cylindrical Pyrex vessel reactor. The UV light source was placed in the middle of vessel. The visible light source was set about 10 cm from the liquid surface of the suspension. The reaction was initiated by switching on the light source after adding the hybrid to dye solutions. The reaction temperature was controlled at 27 °C by recycling the cooling water in a water bath. During the process, at given time intervals, 4 mL of suspension was collected and centrifuged to remove the hybrid, and then analyzed by a UV–Vis spectrophotometer.

The decolorization values of dye solutions were calculated by the following formula:

$$D = \frac{C_0 - C_1}{C_0} \times 100 = \frac{A_0 - A_1}{A_0} \times 100$$

where D is decolorization percent; C_0, A_0 and C_1, A_1 are the concentration and absorbance of dye solution at maximum wavelength before and after irradiation, respectively.

MB adsorption experiments

Adsorption equilibrium experiments were carried out by adding 25 mg HMT–STA into 50 mL MB solution with different concentrations (5–20 mg/L) at room temperature in dark under stirring. The final concentration of MB was defined by UV–Vis spectrometer at 664 nm. The amount of MB adsorbed onto the sorbent in mg/g was calculated using the following equation:

$$q_e = \frac{(C_0 - C_e)V}{m} \quad (1)$$

where C_e is the equilibrium concentration of MB in the solution in mg/L; C_0 is the initial MB concentration in mg/L; m is the amount of sorbent mass in grams, and V is the solution volume in L.

Similar to two previous works (Taghdiri and Zamani 2013; Taghdiri et al. 2015), the isotherm model parameters were determined by nonlinear error functions minimizing using the solver add-in and Microsoft's spreadsheet, Excel. Chi-square statistic (χ^2) was used to evaluate the fitness of isotherm equations to the experimental data.

Kinetic analysis

The kinetic analysis of decolorization was carried out using the pseudo-first-order kinetics, $\ln(C_0/C_t) = kt$, where C_0 is the initial concentration of dye solution; C_t is the concentration of dye solution at time t, and the slope k is the kinetic constant in min^{-1}. The estimated rate constants are listed in Tables 2, 4, and 5. All C_0/C_t values were obtained through the maximum absorption in the whole absorption spectrum in order to plot $\ln(C_0/C_t)$ versus t.

Results and discussion

Characterizations of hybrid

The carbon, hydrogen, and nitrogen elemental analyses (C, 7.42%; H, 1.33%; N, 5.74%) revealed the attachment of seven hexamine molecules to STA and suggested the stoichiometric formula of $[C_6H_{13}N_4]_7[SiW_{12}O_{40}][HSiW_{12}O_{40}].3H_2O$ for HMT–STA hybrid. On the basis of this composition, the calculated elemental analyses are as follows: C, 7.43%; H, 1.45%; N, 5.77%.

The relevant infrared bands of HMT, STA, and HMT–STA are listed in Table 1, while the FTIR spectra were shown in previous work (Taghdiri et al. 2013). The characteristic bands of the polyoxoanions and hexamine are exhibited in the IR spectrum of HMT–STA hybrid. New bands at 1260, 1400, and 1462 cm^{-1} can be attributed to the vibration of the CH_2 of HMT (Jensen 2002). The C–H bending peak at 1400 cm^{-1} shows the organic cation in the hybrid because it can be ascribed to vibration of the CH_2 vicinal to N^+ which is shifted to the lower frequencies upon hybrid formation (Table 1). The strong absorption peaks at 1100–750 cm^{-1} indicate the presence of $SiW_{12}O_{40}^{4-}$ anions with α-Keggin structure. The peaks at 790, 880, 975, and 920 cm^{-1} are ascribed to the stretching modes of the corner sharing of W–O_c–W, edge sharing of W–O_b–W, terminal W–O_d, and Si–O, respectively (Wang and Yang 2010; Zhai et al. 2016).

Table 1 FTIR peak assignment of hexamine (HMT), silicotungstic acid (STA) and HMT–STA hybrid

HMT wave numbers (cm^{-1})	STA wave numbers (cm^{-1})	HMT–STA wave numbers (cm^{-1})	Assignment
	3375	3485	O–H stretching
2955		2950	CH_2 stretching
	1615	1635	O–H scissoring
1457		1462	CH_2 scissoring
1440		1400	CH_2 scissoring
1370			CH_2 wagging
1236		1260	CH_2 rocking
1000			C–N stretching
	950	975	W–O_d scissoring
	899	920	Si–O stretching
	879	880	W–O_b–W stretching
811			C–N stretching
	775	790	W–O_c–W stretching
670			N–C–N bending
	540	528	W–O_c–W stretching
512			N–C–N wagging

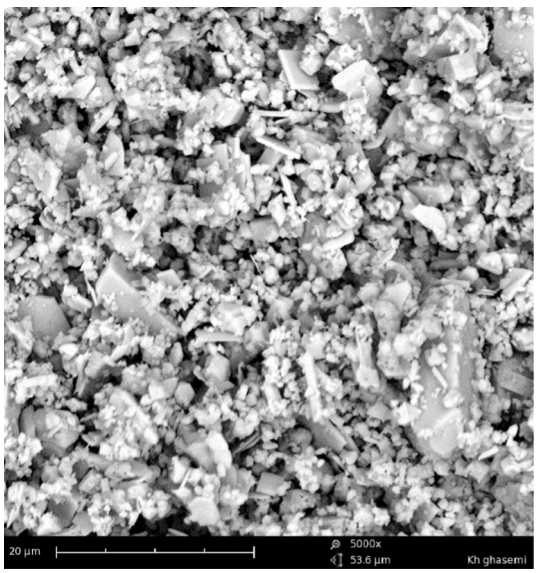

Fig. 1 SEM image of HMT–STA hybrid

The morphology and composition of the hybrid material was characterized by scanning electron microscopy (SEM). The hybrid is composed of microparticles and cubic or rhombus laminas as the SEM image of HMT–STA shows (Fig. 1). The irregular particles with porous morphology and laminas with clear-cut edges and corners are ascribed to STA and HMT, respectively.

In order to confirm the solid structure of hybrid, the powder X-ray diffraction (XRD) patterns of HMT, STA, and HMT–STA are depicted in Fig. 2. Assuming the XRD pattern of HMT–STA and by comparison, the typical peaks of parent STA can be observed ($2\theta = 7.45°$, 8.25°, 25.25°, and 30.15°). The typical peaks at $2\theta = 18.60°$, 31.10°, and 48.35° are from HMT. Therefore, the prime structures of

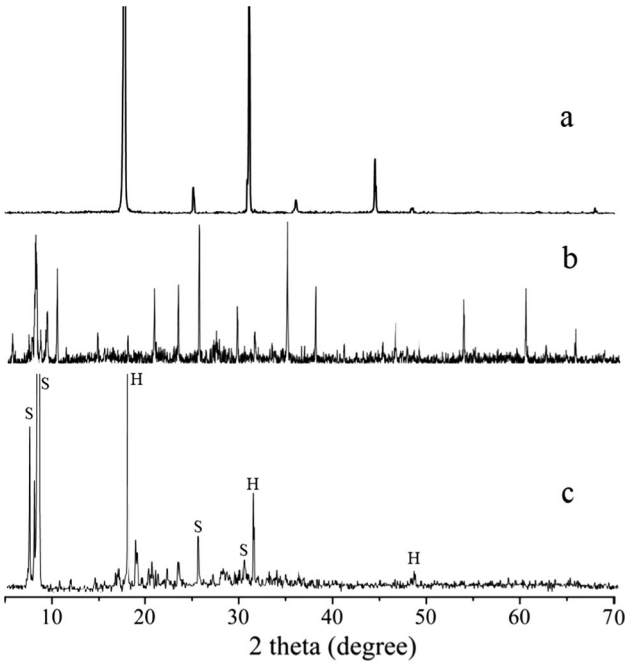

Fig. 2 X-ray diffraction patterns of **a** hexamine, **b** silicotungstic acid, and **c** hexamine–silicotungstate hybrid. The peaks marked as S and H are from silicotungstic acid and hexamine, respectively

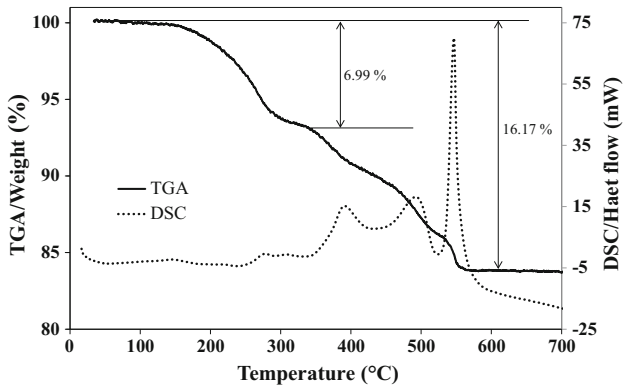

Fig. 3 TGA and DSC curves of HMT–STA hybrid

HMT and STA were preserved intact in the solid structure of hybrid.

The TG and DSC curves of HMT–STA hybrid are shown in Fig. 3. The weight loss of 6.99% and endothermic peak at ca. 150–270 °C are ascribed to the loss of three coordinated water and three hexamine molecules attached to $HSiW_{12}O_{40}^{3-}$ (the calculated value is 7.03%). These weak binding HMT molecules are easily detached from the hybrid and then decomposed. The weak exothermic peaks at 280 and 310 °C are ascribed to the decomposition of these HMT molecules. It has been reported that the hexamine and its complexes are sublimated about 230–290 °C with decomposition at atmospheric pressure (Gusev et al. 1985; Singh et al. 2007; Trzesowska and Kruszynski 2008). Then, the strong binding HMT molecules (i.e., four hexamine molecules attached to $SiW_{12}O_{40}^{4-}$) were released and then decomposed. Therefore, the weak endothermic peak and the next hump-shaped exothermic peaks at 395 and 490 °C correspond to these HMT molecules. In the end, the decomposition of silicotungstate to WO_3 and SiO_2 at about 550 °C took place (Zhang et al. 2016). The whole weight loss of 16.17% is in accordance with the hybrid composition (calculated value = 16.31%).

Hybrid activity for removal and degradation of MB

At first, the efficiency of HMT–STA hybrid for the wastewater treatment was evaluated by removal and degradation of MB. Before the photocatalytic degradation, adsorption of MB on the hybrid was evaluated. The results (the rows of 1–3 of Table 2) showed that hybrid was able to adsorb MB (for instances, see Figs. 4, 5a, S6). Also, the adsorption isotherm of MB adsorbed onto the hybrid was recorded. The most common isotherms for describing solid–liquid sorption systems are the Langmuir, Freundlich, and Toth isotherms. Figure 4 shows the experimental adsorption isotherms for MB/HMT–STA system along with the curve fitted by isotherm models. The isotherm parameters and values of Chi-square are also shown in Table 3. Examination of isotherm plots (Fig. 4) shows that Toth isotherm more accurately describes the sorption behavior of MB on HMT–STA due to exhibiting the lowest value of χ^2. The adsorption data obeyed Toth model exhibiting heterogeneous surface conditions and monolayer adsorption. Therefore, the adsorbate had a high affinity for the surface at low surface coverage. However, as coverage increased, the affinity of the adsorbate for the surface decreased (Fig. 4). The surface charge of the hybrid was negative due to silicotungstate with high electronegative oxygen. Therefore, the interaction between these polyoxoanions and the cationic dye molecules makes a good adsorption toward MB molecules. The order of adsorption isotherm models for MB is Toth > Langmuir > Freundlich (Fig. 6).

The hybrid was then tested as catalyst for the photocatalytic degradation of MB. The HMT–STA exhibits higher photocatalytic activity than the homogenous photocatalyst STA. Compared to adsorption, photocatalytic degradation with HMT–STA displays higher kinetic constant (k) and removal efficiency (Table 2). The kinetic constants of MB (15 mg/L) removal in the visible, UV, and solar photocatalytic process with HMT–STA (0.5 g/L) were 0.1096, 0.0858, and 0.0681 min^{-1}, which are 11.2, 8.7, and 6.9 times higher than that in the adsorption process, respectively. The photocatalytic processes displayed 60.9, 42.9, and 56.7 times higher kinetic constants than the blank experiments, i.e., irradiation without photocatalyst (Table 2; Figs. S1, S4, 7a).

The effect of initial MB concentration

The changes in MB concentration affect the degradation rate of the photocatalytic processes (Table 2). The higher the initial MB concentration is, the longer it takes to reach the same decolorization percent (for instance, compare Figs. 7b, S7). In other words, the rates of MB decolorization decreased with increase in the initial MB concentration (compare the rows of Table 2 in this manner: 5, 9, and 10 for visible; 15, 17, and 18 for sunlight; 24, 25, and 29 for UV). Hence, the complete degradation of a high concentration of MB would require longer time.

Effect of catalyst dosage

The effect of photocatalyst dosage was studied using varying quantities of the hybrid (0.3, 0.6, and 0.8 g/L) for visible and UV light and (0.5 and 1.0 g/L) for sunlight. The decolorization rates of MB increased approximately

Table 2 Adsorption and photodegradation of MB in the presence of HMT–STA

No.	Light	C_{MB} (mg/L)	Catalyst dosage (g/L)	Time (min)	Kinetic constant (min^{-1})	Decolorization (%)
1	Dark (adsorption)	10	0.5	30	0.1120	96.4
2	Dark (adsorption)	15	0.5	300	0.0098	94.5
3	Dark (adsorption)	20	0.5	210	0.0032	43.4
4	Visible	15	0	120	0.0018	21.7
5	Visible	15	0.5	30	0.1096	96.3
6	Visible	15	0.3	110	0.0191	86.7
7	Visible	15	0.6	15	0.2887	95.6
8	Visible	15	0.8	10	0.5594	96.1
9	Visible	10	0.5	5	0.5534	93.7
10	Visible	20	0.5	50	0.0596	96.2
11	Visible	15 + 4 g/L NaCl	0.5	5	0.5212	92.6
12	Visible	15 + 8.5 g/L $NaNO_3$	0.5	5	0.6512	96.1
13	Visible	15 + 14.2 g/L Na_2SO_4	0.5	10	0.3416	96.9
14	Solar	15	0	180	0.0012	21.3
15	Solar	15	0.5	40	0.0681	98.9
16	Solar	15	1.0	30	0.1242	97.6
17	Solar	10	0.5	30	0.0797	90.8
18	Solar	20	0.5	150	0.0242	97.1
19	Solar	20	0.5	30	0.0242	39.8
20	Solar	15 + 4 g/L NaCl	0.5	40	0.0728	96.8
21	Solar	15 + 8.5 g/L $NaNO_3$	0.5	40	0.0750	96.7
22	Solar	15 + 14.2 g/L Na_2SO_4	0.5	40	0.1053	98.8
23	UV	10	0	175	0.0020	28.8
24	UV	10	0.5	15	0.2062	94.7
25	UV	15	0.5	70	0.0858	96.5
26	UV	15	0.3	240	0.0071	78.4
27	UV	15	0.6	30	0.1418	97.8
28	UV	15	0.8	15	0.2092	95.8
29	UV	20	0.5	70	0.0407	92.4
30	UV	20	0.5	20	0.0407	68.5
31	UV	15 + 4 g/L NaCl	0.5	17	0.1838	96.3
32	UV	15 + 8.5 g/L $NaNO_3$	0.5	10	0.3409	96.8
33	UV	15 + 14.2 g/L Na_2SO_4	0.5	5	0.7913	97.8
34	UV	15 (in seawater)	0.5	5	0.4741	90.7
35	Visible	15 (in seawater)	0.5	5	0.6189	95.5

proportional with increase in the HMT–STA concentration (compare the rows of Table 2 in this manner: 6–8 for visible; 15 and 16 for sunlight; 26–28 for UV).

The effect of different ions

The effect of some common ions on the photocatalytic degradation of MB was studied considering some different ions in real wastewater. The results of the effect of added salts (the rows of 11–13, 20–22, and 31–33 of Table 2) showed that 0.1 M NaCl, $NaNO_3$, and Na_2SO_4 increased the degradation rate of MB (compare Figs. S3, S5, S8 with Figs. S2, 6a, S7, respectively).

Photocatalytic activity for MO degradation

To further investigate the activity of HMT–STA hybrid, it was used for photodecomposition of MO under UV, visible, and sunlight irradiation. Before the photocatalytic degradation of MO, the adsorption process was studied in acidic aqueous solution (pH = 2.5). HMT–STA cannot adsorb MO because MO is a neutral form in pH 2.5 (the

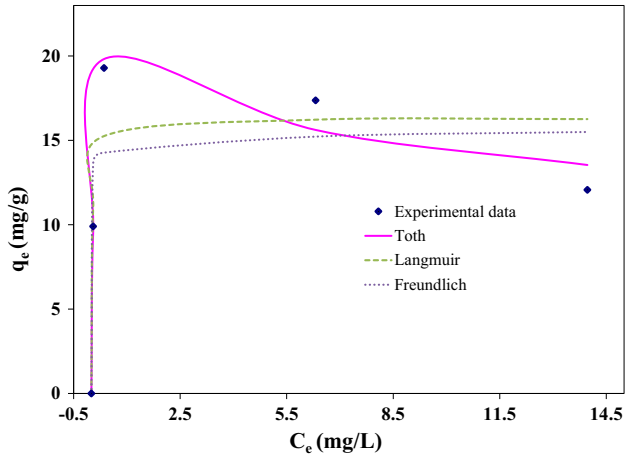

Fig. 4 Langmuir, Freundlich, and Toth isotherms for the adsorption of MB by HMT–STA hybrid ($V = 50$ mL, sorbent dosage = 0.5 g/L, pH = without adjustment and $T = 25$ °C)

Table 3 Parameters of the isotherm models for the adsorption of MB onto HMT–STA

Model	Equation	Parameter	Value	χ^2
Toth	$q_e = \frac{K_t C_e}{(a_t + C_e)^{1/t}}$	K_t	22.887	0.384
		a_t	0.119	
		$1/t$	1.195	
Langmuir	$q_e = \frac{q_m K_a C_e}{1 + K_a C_e}$	q_m	16.288	2.335
		K_a	41.336	
Freundlich	$q_e = K_F C_e^{1/n}$	K_F	14.602	3.859
		$1/n$	0.022	

adsorption of MO is about 5%). All results of UV, visible, and sunlight irradiation on MO photodegradation are shown in Table 4 and Figs. 8, 9, and supplementary materials in Figures S9 and S12. It can be seen that UV and sunlight are able to degrade MO with HMT–STA photo-

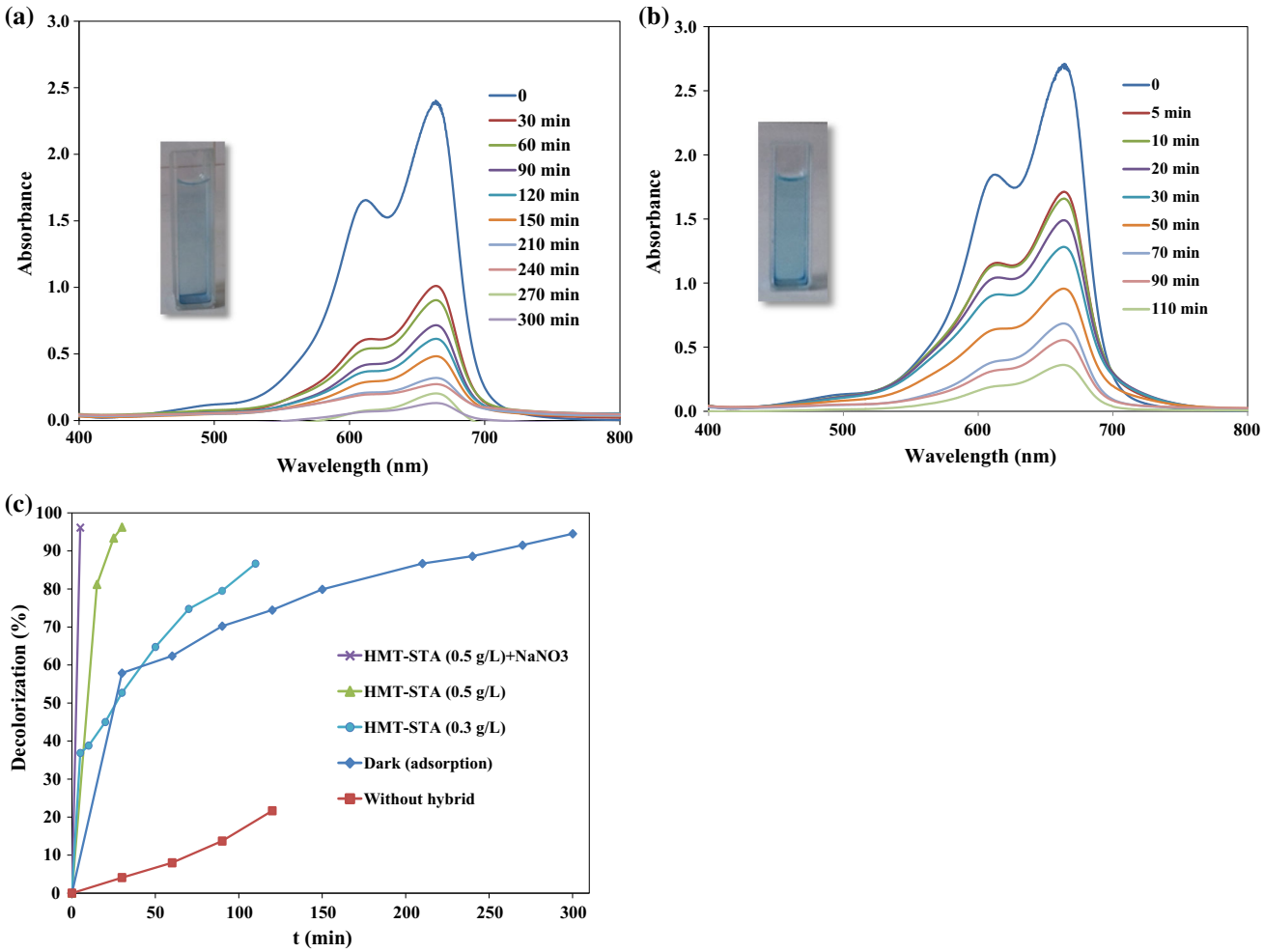

Fig. 5 UV–Vis absorption spectra of the MB solution (15 mg/L) **a** during the adsorption on HMT–STA (0.5 g/L) in the dark, **b** during the photodegradation under visible light irradiation in the presence of the HMT–STA (0.3 g/L), and **c** changes in decolorization percent of MB solution versus time. *Inset* the color change in dye solution after irradiation

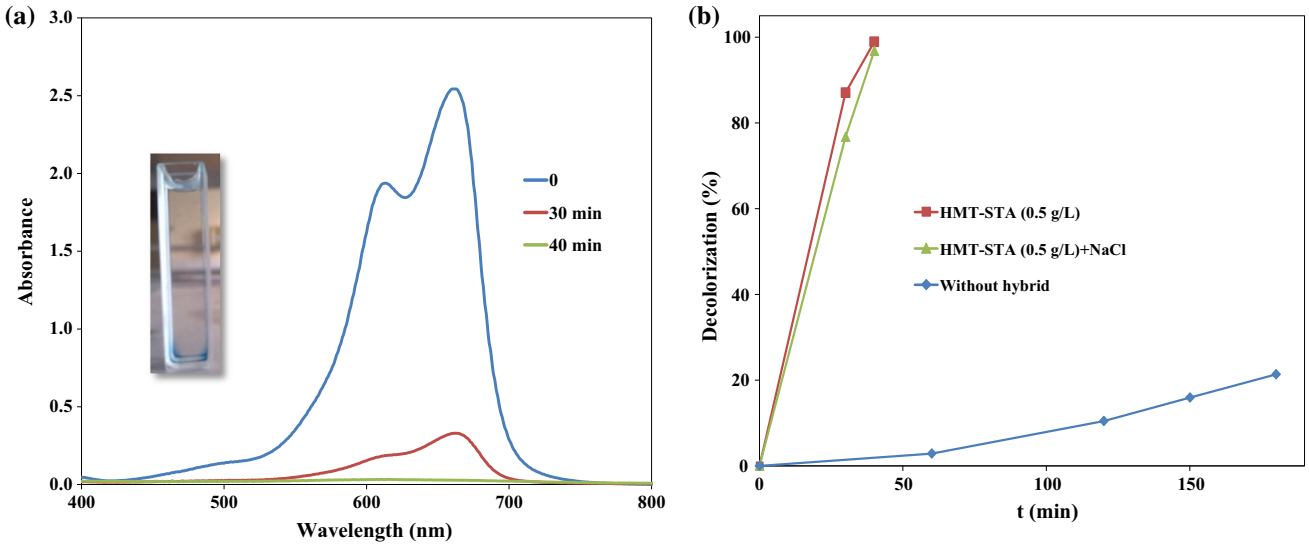

Fig. 6 **a** UV–Vis absorption spectra of the MB solution (15 mg/L) during the photodegradation under sunlight irradiation in the presence of the HMT–STA (0.5 g/L) and **b** changes in decolorization percent of MB solution versus time. *Inset* the color change in dye solution after irradiation

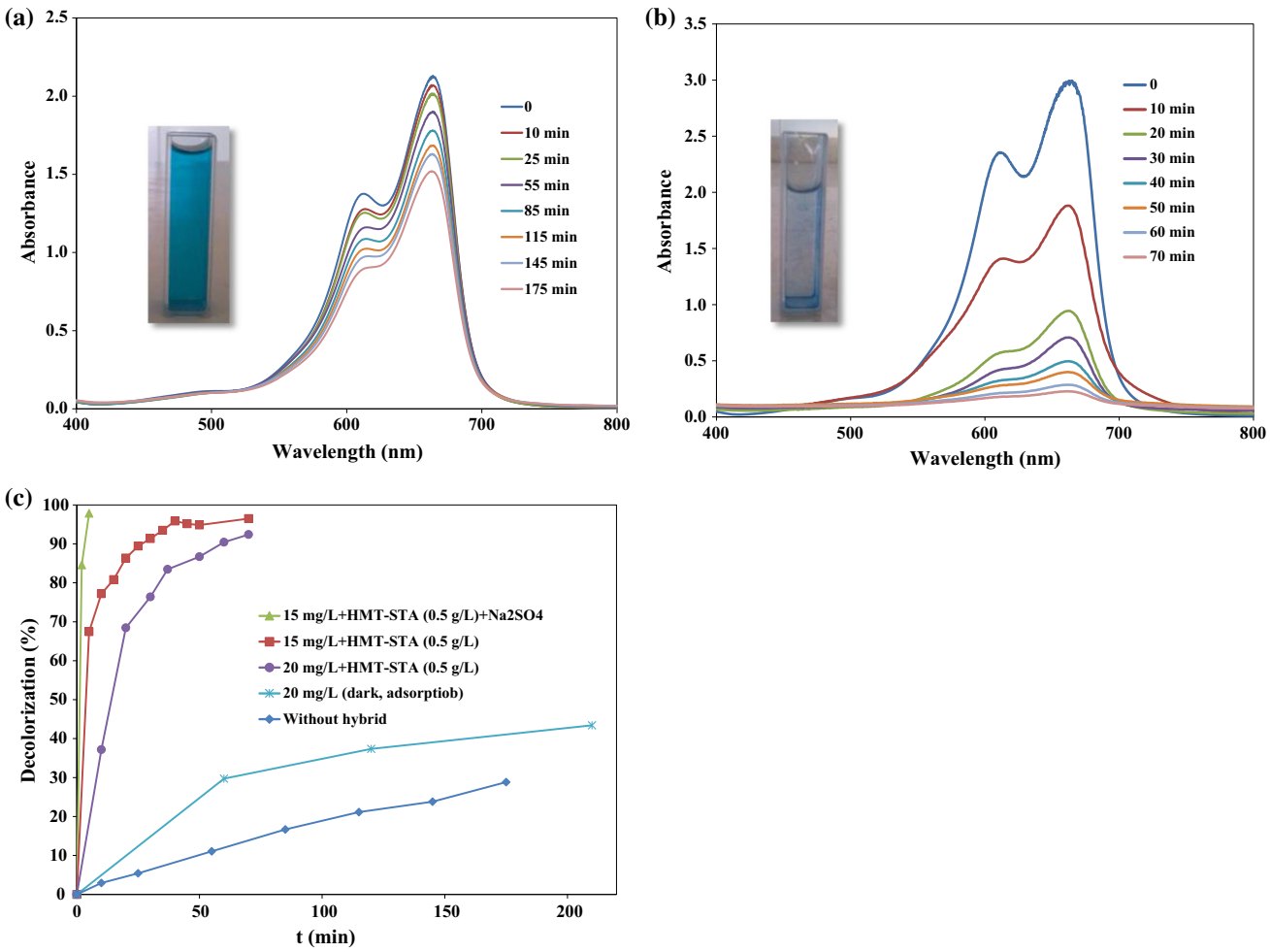

Fig. 7 UV–Vis absorption spectra of MB during the photodegradation under UV light irradiation: **a** the MB solution (10 mg/L) without the HMT–STA hybrid, **b** the MB solution (20 mg/L) in the presence of the HMT–STA (0.5 g/L) and **c** changes in decolorization percent of MB solution versus time. *Inset* the color change in dye solution after irradiation

Table 4 Photodegradation of MO in the presence of HMT–STA

No.	Light	C_{MO} (mg/L)	Catalyst dosage (g/L)	H_2O_2 dosage (μL)	Time (min)	pH	Kinetic constant (min^{-1})	Decolorization (%)
1	Visible	10	0.5	0	120	2.5	0	0
2	UV	10	0	0	115	2.5	0.0046	35.9
3	UV	5	0.4	0	85	2.5	0.0250	85.1
4	UV	10	0.5	0	120	2.5	0.0096	68.5
5	UV	10	0.6	0	90	2.5	0.0271	93.2
6	UV	20	0.4	0	120	2.5	0.0048	46.8
7	UV	10 + 4 g/L NaCl	0.5	0	120	2.5	0.0068	37.9
8	UV	10 + 8.5 g/L $NaNO_3$	0.5	0	120	2.5	0.0089	67.1
9	UV	10 + 14.2 g/L Na_2SO_4	0.5	0	120	2.5	0.0020	29.5
10	Solar	10	0	3	150	2.5	0.0019	23.2
11	Solar	10	0.5	0	180	2.5	0.0029	41.5
12	Solar	10	0.75	0	180	2.5	0.0032	47.2
13	Solar	10	1	0	180	2.5	0.0059	65.0
14	Solar	10	0.5	3	180	2.5	0.0031	41.9
15	Solar	10	0.75	3	180	2.5	0.0053	60.1
16	Solar	10	1	3	180	2.5	0.0066	66.9
17	Solar	10	0.5	6	180	2.5	0.0041	54.9
18	Solar	5	0.5	0	150	2.5	0.0101	80.2
19	Solar	15	0.5	0	150	2.5	0.0024	30.2
20	Solar	10	0.5	0	180	1.6	0.0030	40.7
21	Solar	10	0.5	0	180	3.6	0.0026	37.4
22	Solar	10	0.5	0	180	4.6	0.0006	8.6
23	Solar	10	0.5	0	180	6.1	0.0006	7.9

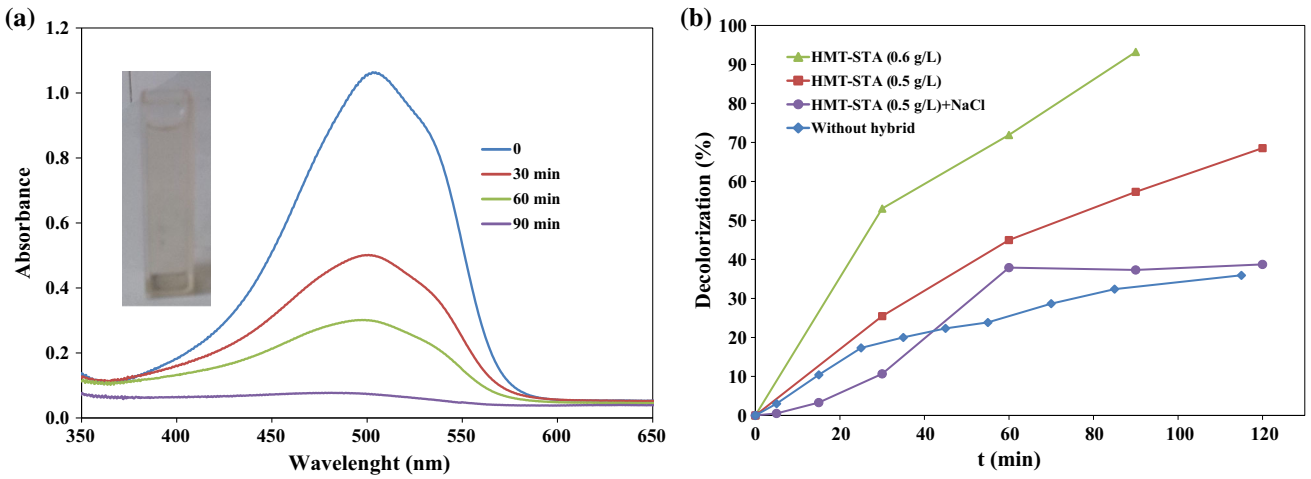

Fig. 8 **a** UV–Vis absorption spectra of the MO solution (10 mg/L, pH = 2.5) during the photodegradation under UV light irradiation in the presence of the HMT–STA (0.6 g/L) and **b** changes in decolorization percent of MO solution versus time. *Inset* the color change in dye solution after irradiation

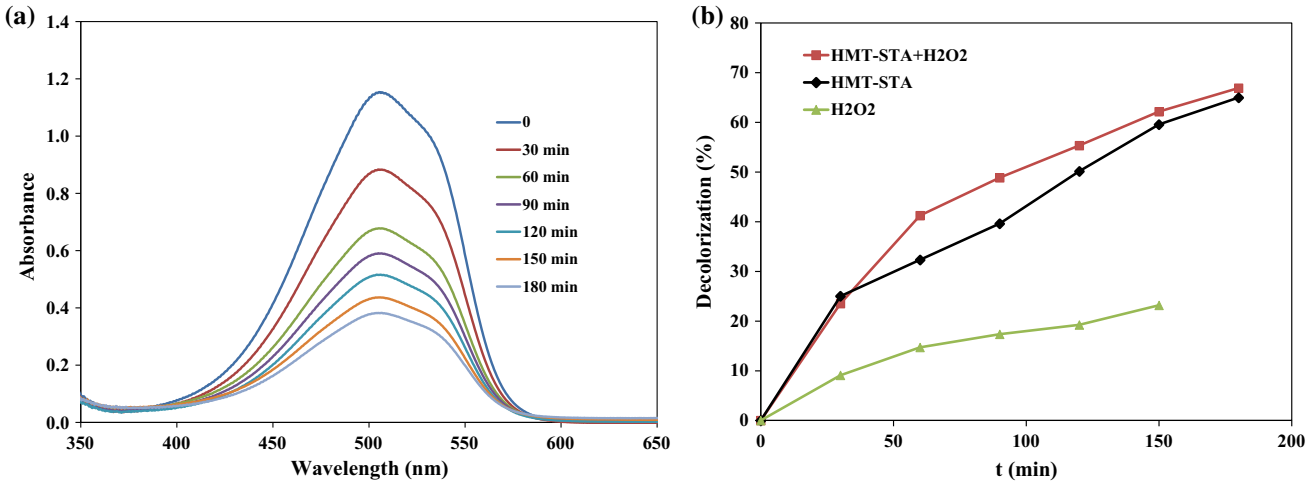

Fig. 9 **a** UV–Vis absorption spectra of the MO solution (10 mg/L, pH = 2.5) during the photodegradation under sunlight irradiation in the presence of the HMT–STA (1 g/L) and 3 μL H_2O_2 and **b** changes in decolorization percent of MO solution versus time

catalyst. Similar to MB photodegradation, the rates of MO decolorization decreased with increase in the initial MO concentration (compare the rows of Table 4 in this manner: 3 and 6 for UV; 11, 18, and 19 for sunlight) and increased with increase in the HMT–STA concentration (compare the rows of Table 4 in this manner: 4 and 5 and corresponding Figs. S10 and 8a for UV; the rows of 11–16 for sunlight).

Effect of the solution pH

Table 4 (the rows of 11 and 20–23) shows the kinetic constants and decolorization percent obtained at different pH values after 180 min in the presence of 0.5 g/L HMT–STA under sunlight irradiation. The highest decolorization efficiency was obtained at pH of 1.6–2.5. At higher pH values, the efficiency of the process decreased because MO is anionic and because of electrostatic repulsion with the negatively charged surface of HMT–STA.

Effect of added H_2O_2

The effect of hydrogen peroxide on the rate and percent of MO decolorization in the presence of the same amount of hybrid, pH, and time under sunlight irradiation is shown in Table 4 (the rows of 14–17). The addition of hydrogen peroxide caused an increase in the rate and percent of decolorization (compare the rows 11, 14, and 17 in Table 4; Figs. 9a, S13). This could be attributed to the $^{\cdot}OH$ radicals formed through reduction of H_2O_2 by reduced HMT–STA (Taghdiri et al. 2013) that could further contribute to the oxidation of the azo dye (the orange arrows above scheme 1).

The effect of different ions

The effect of some common ions on the photocatalytic UV degradation of MO is shown in the rows of 7–9 (Table 4). The decolorization rate of MO declined under 0.1 M NaCl, $NaNO_3$, and Na_2SO_4 (Figure S11). The affecting extent followed the order $SO_4^{2-} > Cl^- > NO_3^-$. This effect may be attributed to the quenching of hydroxyl radicals by these ions (Yin et al. 2009) (see "Mechanism of photodegradation" section).

Photocatalytic activity for a mixture of MB and MO degradation

The real wastewater can not only contain a single component. Hence, the mixture of MB and MO was selected to explore the ability of the hybrid in the degradation of mixed dye molecules. Table 5 shows the kinetic constants and decolorization percent of the mixed solutions of MB and MO in the presence of 0.5 g/L of the hybrid in pH 7.5 (without adjustment) under visible light irradiation. The results clearly confirmed that the hybrid degrades both MB and MO dyes, but the rate and percent of MO decolorization are lower than those of MB. It is interesting that visible light is able to degrade MO in the mixed solutions in the presence of HMT–STA hybrid (Fig. 10), while it could not degrade alone MO (Table 4, the first row). Moreover, the efficiency of MO degradation increased with increase in the initial MO concentration in the same amount of MB in the mixture. Because HMT–STA has a surface negative charge due to STA anions, the cationic MB molecules are preferentially adsorbed on it. Then, the surface of the

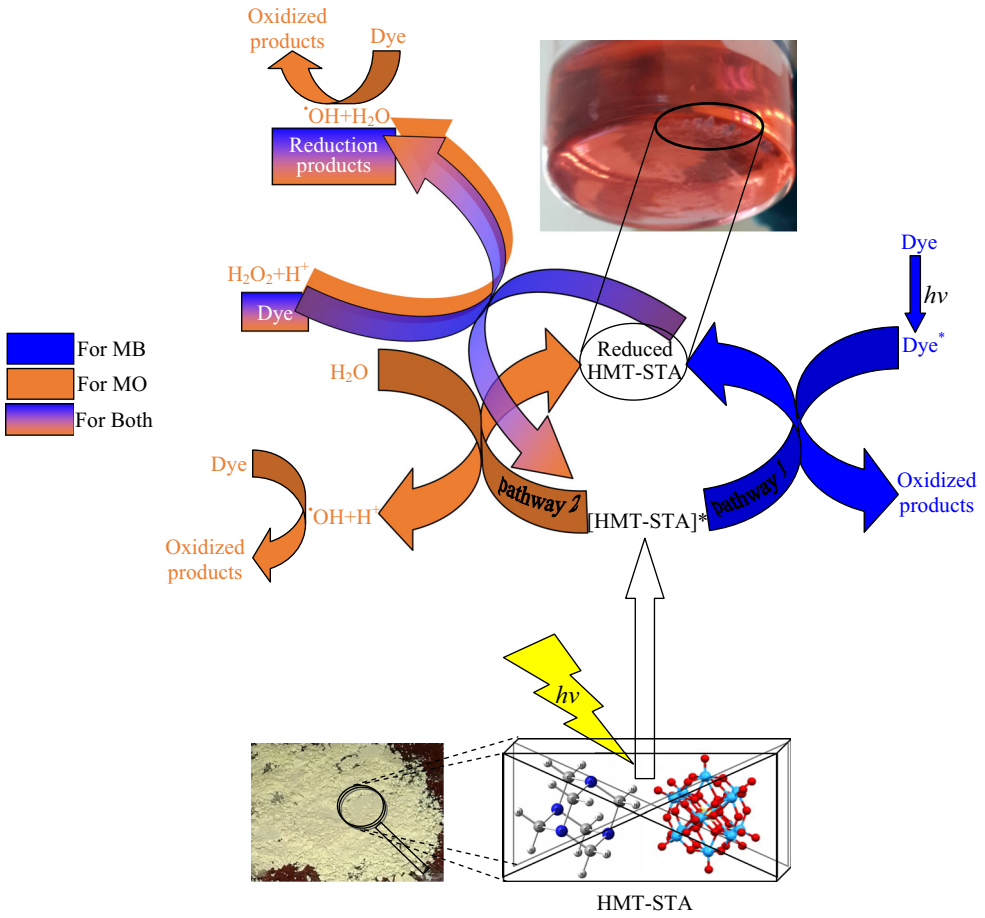

Scheme 1 Proposed mechanism for photodegradation of dyes by HMT–STA hybrid

Table 5 Visible light degradation of mixture of MB and MO

Light	$C_{MB,\ MO}$ (mg/L)	Catalyst dosage (g/L)	Time (min)	pH	Kinetic constant for MB, MO (min^{-1})	Decolorization of MB, MO (%)
Visible	15, 5	0.5	25	7.5	0.4536, 0.1002	97.4, 39.4
Visible	15, 10	0.5	25	7.5	0.4250, 0.1242	96.6, 47.0
Visible	15, 15	0.5	60	7.5	0.0203, 0.0220	86.8, 78.4
Visible	15, 10	0.5	155	2.5	0.0067, 0.0009	77.8, 23.4

hybrid possessing a slightly positive charge adsorbs the anionic MO molecules. Indeed, the higher adsorption of MO increases the efficiency of photodegradation. Hence, the decrease in pH decreases the efficiency of degradation (Table 5, the last row) because MO is neutral in pH 2.5.

Mechanism of photodegradation

A proposed photodegradation mechanism is deduced that irradiation of the HMT–STA hybrid with light (*hv*) results in the formation of the excited state ([HMT–STA]*, see Scheme 1) without significant change on its molecular structure:

$$\text{HMT}-\text{STA} + hv \rightarrow [\text{HMT}-\text{STA}]^* \quad (2)$$

This excited state of the hybrid results from the oxygen to metal charge transfer band of STA (Dolbecq et al. 2012). This phenomenon can be reinforced by the electron transfer between HMT and STA resulting from the strong interaction between HMT and STA species in the hybrid. The shift of the IR bands reflects the strong interaction in the HMT–STA hybrid (Table 1). The [HMT–STA]* is a

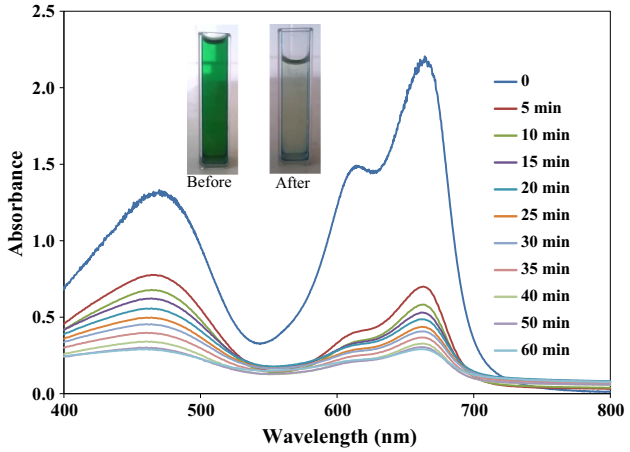

Fig. 10 UV–Vis absorption spectra of the mixed solution of MB and MO (each dye 15 mg/L) during the photodegradation under visible light irradiation in the presence of the HMT–STA (0.5 g/L) and corresponding digital images of the mixed solution before and after irradiation

strong oxidant able to oxidize and, most often, mineralize organic dyes. There are two pathways through which the excited HMT–STA is reduced: reaction with excited organic dye in aqueous solution (pathway 1 in scheme 1) through reactions 3–5,

$$\text{Dye} + h\nu \rightarrow \text{Dye}^{*} \quad (3)$$

$$[\text{HMT}-\text{STA}]^{*} + \text{Dye}^{*} \rightarrow [\text{HMT}-\text{STA}](e^{-}) + \text{Dye}^{+\cdot} \quad (4)$$

$$\text{Dye}^{+\cdot} \rightarrow \text{decomposition into colorless products} \quad (5)$$

and reaction through formation of $^{\cdot}$OH radicals from the reaction with H_2O (Streb 2012) (pathway 2 in scheme 1) through reaction 6,

$$[\text{HMT}-\text{STA}]^{*} + H_2O \rightarrow [\text{HMT}-\text{STA}](e^{-}) + {}^{\cdot}\text{OH} + H^{+} \quad (6)$$

The organic dye is oxidized directly in pathway 1 and indirectly by $^{\cdot}$OH radicals in pathway 2. The HMT–STA is reduced to a blue colored solid (see the picture of beaker in Scheme 1 and reaction 4). The reduced hybrid can be re-oxidized by the reduction of dye (see double-colored arrows in scheme 1) through reactions 7 and 8,

$$[\text{HMT}-\text{STA}](e^{-}) + \text{Dye} \rightarrow [\text{HMT}-\text{STA}] + \text{Dye}^{-} \quad (7)$$

$$\text{Dye}^{-} \rightarrow \text{reduction products} \quad (8)$$

or by H_2O_2, if it is added, which undergoes reductive activation through the formation of $^{\cdot}$OH radicals,

$$[\text{HMT}-\text{STA}](e^{-}) + H_2O_2 + H^{+} \rightarrow [\text{HMT}-\text{STA}] + {}^{\cdot}\text{OH} + H_2O \quad (9)$$

These species are strong oxidants capable of initiating further oxidation of dye (see orange arrows above scheme 1),

$$\text{Dye} + {}^{\cdot}\text{OH} \rightarrow \text{oxidized products} \quad (10)$$

The mechanism of MB degradation took place through pathway 1, i.e., dye-sensitized degradation. Dye-sensitized degradations take place where there exists an interaction between dye and photocatalyst (Chen et al. 2004). In the case of the cationic MB molecules, there was an interaction with polyoxoanions of HMT–STA hybrid. Therefore, the process of degradation involved absorption of light by MB molecules followed by charge injection into the hybrid and then oxidative degradation of MB (follow blue arrows of scheme 1). The mechanism of MO degradation took place through pathway 2, i.e., indirect oxidation by $^{\cdot}$OH radicals (follow orange arrows of scheme 1) because neutral MO molecules (in pH = 2.5) were not strongly adsorbed on the negatively charged surface of hybrid unlike MB. It has been reported that the $^{\bullet}$OH-mediated indirect oxidation is an order of magnitude slower than direct elimination (Troupis et al. 2009). Hence, the photodegradation kinetic constant of pure MO and MO in the binary MB/MO mixture was slower than that of MB (Tables 2, 4, 5).

The mechanisms assigned to MB and MO degradation were compatible with the effect of salt addition ("The effect of different ions" section and "The effect of different ions" section). The decrease in MO degradation resulted from the quenching effect of added ions on $^{\cdot}$OH radicals contributing to oxidation of MO. However, the effect of these ions on MB degradation was unlike MO because the $^{\cdot}$OH radicals did not chip in oxidation of MB.

The mechanism of the photocatalytic process under UV and visible irradiation is different. The UV light creates the exited hybrid that can oxidize MB molecules. However, the visible light irradiation will not create the exited hybrid, but it induces the adsorbed MB to act as sensitizer. Meanwhile, the hybrid accepts the electrons from the excited MB and reduces. Hence, the photodegradation of alone MO did not occur under visible light (Table 4, the first row) because of no adsorption of neutral MO on the surface of the HMT–STA hybrid. However, the photodegradation of the MO mixed with MB solution occurred because of adsorption of anionic MO on positive surface of the HMT–STA–MB in pH 7.5 (Table 5).

The reusability of hybrid catalyst

The reusability and stability of the catalysts is an important characteristic in catalytic technology considering economic feasibility. Thus, the reusability of hybrid catalyst in the photodegradation of MB under UV light irradiation was investigated. Successive photocatalytic experiments were performed with the solids recycled from the solution by centrifugation. The decolorization efficiency still reached 73.6% after three

Table 6 Comparison of photodegradation of MB and MO by using STA, different hybrid catalysts containing STA reported in the literature and STA-HMT

Catalysts	Light	C_{dye} (mg/L)	Catalyst dosage (g/L)	Time (min)	Decolorization (%)	References
$SiW_{12}O_{40}^{4-}$ (homogeneous catalyst)	Vis.	MO (4.5)[a]	8.89	140	21	Wang and Yang (2010)
$KH[SiW_{12}O_{40}][Ni(H_2O)_6]CB[6]\cdot 7H_2O$	Vis.	MO (10)	0.5	120	93.6	Dolbecq et al. (2012)
$[H_2bimb][Cu\ bimb][SiW_{12}O_{40}]\cdot 2H_2O$	UV	MB (10)	0.125	90	90[a]	Hao et al. (2015)
$[Cu_2(4\text{-atrz})_6(SiW_{12}O_{40})(H_2O)]\cdot 6H_2O$	UV	MB (6)	1.67	60	98.22	Wang et al. (2015a)
$[Cu_2(4\text{-atrz})_6(SiW_{12}O_{40})(H_2O)]\cdot 6H_2O$	UV	MO (6)	1.67	180	5.75	Wang et al. (2015a)
$[Cu_2(2,2'\text{-tmbpt})_2(SiW_{12}O_{40})]\cdot 9H_2O$	UV	MB (16)	0.15	120	41	Kan et al. (2014)
$Cu_2(2,3'\text{-tmbpt})_2(SiW_{12}O_{40})]\cdot 6H_2O$	UV	MB (16)	0.15	120	51	Kan et al. (2014)
$[Cu_2(2,4'\text{-tmbpt})_2(SiW_{12}O_{40})(H_2O)_2]\cdot 6.5H_2O$	UV	MB (16)	0.15	120	58	Kan et al. (2014)
$[Cu_2(4,4'\text{-tmbpt})_2(SiW_{12}O_{40})(H_2O)_4]\cdot 13.5H_2O$	UV	MB (16)	0.15	120	74	Kan et al. (2014)
$[(CH_3)_2NH_2]_2[ZnL_2(SiW_{12}O_{40})]\cdot 7DMF\cdot 13H_2O$	Vis.	MB (10)	0.75	17	95	Ou et al. (2015)
$[(H_2toym)_2(SiW_{12}O_{40})]\cdot 6H_2O$	UV	MB (3.2)	0.35	120	80.4	Guo et al. (2013)
$[Cu^{I}_2Cu^{II}(BBPTZ)_6][SiW_{12}O_{40}]\cdot 12H_2O$	UV	MB (10)	0.17	90	97.5	Hao et al. (2014)
$[Ni(BBPTZ)_2(H_2O)][H_2SiW_{12}O_{40}]\cdot 11H_2O$	UV	MB (10)	0.17	90	96.9	Hao et al. (2014)
$[Ni_2(BBPTZ)_4(H_2O)_2][SiW_{12}O_{40}]\cdot 3H_2O$	UV	MB (10)	0.17	90	94.1	Hao et al. (2014)
$[Ag(phen)_2]_2(Agphen)_2SiW_{12}O_{40}$	UV	MB (20)	0.5	210	70.25	Pang et al. (2015)
$[Cu_2(bpypi)_2(SiW_{12}O_{40})(H_2O)_6]\cdot H_2O$	UV	MB (10)[a]	150[b]	210	90.6	Wang et al. (2015b)
$[Cu_2(bpypi)_2(SiW_{12}O_{40})(H_2O)_6]\cdot H_2O$	Vis.	MB (10)[a]	150[b]	210	71.9	Wang et al. (2015b)
$[Zn_{12.5}(trz)_{17}(H_2O)_7(SiW_{12}O_{40})_2]\cdot 2H_2O$	UV	MB (16)	0.3	120	91.0	Zhou et al. (2016)
$[Zn_{12.5}(trz)_{17}(H_2O)_7(SiW_{12}O_{40})_2]\cdot 2H_2O$	UV	MO (16)	0.3	120	78	Zhou et al. (2016)
$[Pb_2(dpdo)_5(H_2O)_3(SiW_{12}O_{40})]\cdot H_2O$	UV	MB (16)	0.3	120	94.3	Zhou et al. (2016)
$[Pb_2(dpdo)_5(H_2O)_3(SiW_{12}O_{40})]\cdot H_2O$	UV	MO (16)	0.3	120	88.6	Zhou et al. (2016)
$[Cu_2(DIBA)_4](H_4SiW_{12}O_{40})\cdot 6H_2O$	UV	MB (10)	1.67	180	64.7	Wang et al. (2016)
$[C_6H_{13}N_4]_7[SiW_{12}O_{40}][HSiW_{12}O_{40}].3H_2O$	UV	MO (10)	0.6	90	93.2	This work
$[C_6H_{13}N_4]_7[SiW_{12}O_{40}][HSiW_{12}O_{40}].3H_2O$	Solar	MO (5)	0.5	150	80.2	This work
$[C_6H_{13}N_4]_7[SiW_{12}O_{40}][HSiW_{12}O_{40}].3H_2O$	UV	MB (15)	0.6	30	97.8	This work
$[C_6H_{13}N_4]_7[SiW_{12}O_{40}][HSiW_{12}O_{40}].3H_2O$	Solar	MB (15)	0.5	40	99.0	This work
$[C_6H_{13}N_4]_7[SiW_{12}O_{40}][HSiW_{12}O_{40}].3H_2O$	Vis.	MB (15)	0.5	30	96.3	This work

CB[6] = cucurbit[6]uril, bimb = 1,4-bis(1 imidazolyl)benzene, 4-atrz = 4-amino-1,2,4-triazole, 2,2′-tmbpt = 1-((1*H*-1,2,4-triazol-1-yl)methyl)-3,5-bis(2-pyridyl)-1,2,4-triazole, 2,3′-tmbpt = 1-((1*H*-1,2,4-triazol-1-yl)methyl)-3-(3-pyridyl)-5-(2-pyridyl)-1,2,4-triazole, 2,4′-tmbpt = 1-((1*H*-1,2,4-triazol-1-yl)methyl)-3-(4-pyridyl)-5-(2-pyridyl)-1,2,4-triazole, 4,4′-tmbpt = 1-((1*H*-1,2,4-triazol-1-yl)methyl)-3,5-bis(4-pyridyl)-1,2,4-triazole, L = 1,1′-methylenebis(3-(4-carboxyphenyl)-1*H*-imidazol-3-ium), toym = 2,4,6-tris[1-(4 oxidroxypyridinium)-yl-methyl]-mesitylene, BBPTZ = 4,4′-bis(1,2,4-triazol-1-ylmethyl)biphenyl, phen = 1,10-phenanthroline, bpypi = N,N′-bis(3-pyridinecarboxamide)-piperazine, trz = 1,2,4-triazole, dpdo = 4,4′-bipyridine-N,N′-dioxide, DIBA = 3,5-di(1*H*-imidazol-1-yl) benzoic acid)

[a] Value was estimated from original figure of the reference

[b] mg, volume of solution was unknown

rounds of recycle (Figure S14), indicating that the catalyst had good repeated efficiency. The reduction in catalytic activity after reusing for three cycles might be related to the slight loss of catalyst in the process of recycle. Further studies are required to incorporate the hybrid on the surface of porous materials in order to access easy and efficient separation.

Comparison with other organic hybrids of STA

To compare the photocatalytic efficiency of HMT–STA hybrid with other organic hybrids of STA reported in the literature, the findings are summarized in Table 6. The advantages of the present photocatalytic system are that it does not use expensive organic moieties (see footnotes of

Table 6) in the hybrid preparation, it has higher rate of decolorization and shows photocatalytic behavior under visible light and sunlight in addition to UV light.

Application in natural seawater

To obtain further insight into the photocatalytic behavior of HMT–STA hybrid in a practical application, natural seawater was used instead of distilled water to prepare the simulated dye solution. The seawater was collected from Persian Gulf (Bushehr, Iran). Any suspended particles were removed from the seawater and then the MB sample was added. The results showed that after 5-min illumination of visible and UV light, 95.5 and 90.7% of MB were removed, respectively (the last two rows of Table 2). These results are compatible with the results using distilled water in the presence of added salts ("The effect of different ions" section). The presence of natural salts in seawater accelerated photodegradation of MB.

Conclusion

In summary, a novel water-insoluble organic–inorganic hybrid constructed from hexamine and silicotungstic acid was synthesized and characterized. The hexamine–silicotungstate hybrid is a good heterogeneous photocatalyst in the degradation of MB and MO organic dyes and their binary mixtures under UV, visible, and sunlight irradiation. It is particularly interesting that the single components of the hybrid are either catalytically inactive toward the degradation of organic dyes under visible light irradiation or show very low activity. The MB is removed via combination of adsorption and photocatalytic degradation under visible light. The visible light may degrade MO in the mixed solution in the presence of hybrid, while it does not degrade alone MO. The MB and MO degradation proceeded through direct oxidation by hybrid and indirect oxidation by $^{\cdot}OH$ radicals, respectively.

This study proved that polyoxometalate–organic hybrids can act as a promising effective photocatalyst for visible light and sunlight degradation of aqueous organic pollutants in addition to the UV degradation.

Acknowledgements The authors express their appreciation to Payame Noor University and Sina Chemical Industries Company.

References

Afkhami A, Saber-Tehrani M, Bagheri H (2010) Modified maghemite nanoparticles as an efficient adsorbent for removing some cationic dyes from aqueous solution. Desalination 263:240–248. doi:10.1016/j.desal.2010.06.065

Alamdari A, Tabkhi F (2004) Kinetics of hexamine crystallization in industrial scale. Chem Eng Process 43:803–810

Baghernejad A, Yaghoubi M (2010) Exergy analysis of an integrated solar combined cycle system. Renew Energy 35:2157–2164

Chen C, Zhao W, Lei P, Zhao J, Serpone N (2004) Photosensitized degradation of dyes in polyoxometalate solutions versus TiO_2 dispersions under visible-light irradiation: mechanistic implications. Chem Eur J 10:1956–1965

Deng Y et al (2016a) Enhanced visible light photocatalytic performance of polyaniline modified mesoporous single crystal TiO_2 microsphere. Appl Surf Sci 387:882–893

Deng Y et al (2016b) Facile fabrication of a direct Z-scheme Ag_2CrO_4/gC_3N_4 photocatalyst with enhanced visible light photocatalytic activity. J Mol Catal A Chem 421:209–221

Dolbecq A, Mialane P, Keita B, Nadjo L (2012) Polyoxometalate-based materials for efficient solar and visible light harvesting: application to the photocatalytic degradation of azo dyes. J Mater Chem 22:24509–24521

Fetterolf ML, Patel HV, Jennings JM (2003) Adsorption of methylene blue and acid blue 40 on titania from aqueous solution. J Chem Eng Data 48:831–835

Gamelas JA, Cavaleiro AM, de Matos Gomes E, Belsley M, Herdtweck E (2002) Synthesis, properties and photochromism of novel charge transfer compounds with Keggin anions and protonated 2,2′-biquinoline. Polyhedron 21:2537–2545

García-López EI, Marcì G, Palmisano L (2016) Heteropolyacid-based heterogeneous photocatalysts for environmental application. In: Heterogeneous photocatalysis. Springer, Berlin, pp 63–107

Giri SK, Das NN, Pradhan GC (2011) Synthesis and characterization of magnetite nanoparticles using waste iron ore tailings for adsorptive removal of dyes from aqueous solution. Colloid Surf Physicochem Eng Asp 389:43–49. doi:10.1016/j.colsurfa.2011.08.052

Guo J, Yang J, Liu Y-Y, Ma J-F (2013) Two new polyoxometalate-templated supramolecular compounds constructed by a new tridentate ligand 2,4,6-tris [1-(4-oxidroxypyridinium)-ylmethyl]-mesitylene. Inorg Chim Acta 400:51–58

Gusev EA, Dalidovich SV, Krasovskaya LI (1985) Investigation of urotropine thermal decomposition reaction in self-generated atmosphere by means of thermal analysis method. Thermochim Acta 93:21–24. doi:10.1016/0040-6031(85)85006-1

Hao XL, Ma YY, Zhou WZ, Zang HY, Wang YH, Li YG (2014) Polyoxometalate-based entangled coordination networks induced by an extended bis (triazole) ligand. Chem Asian J 9:3633–3640

Hao HF, Zhou WZ, Zang HY, Tan HQ, Qi YF, Wang YH, Li YG (2015) Keggin-type polyoxometalate-based metal-organic networks for photocatalytic dye degradation. Chem Asian J 10:1676–1683

Hazra DK, Chatterjee R (2013) In situ solid state polymerization and characterization of poly(*N*-vinylcarbazole) encapsulated Keggin type polyoxometalate nanocomposite. J Mol Struct 1045:139–144

He T, Yao J (2006) Photochromism in composite and hybrid materials based on transition-metal oxides and polyoxometalates. Prog Mater Sci 51:810–879. doi:10.1016/j.pmatsci.2005.12.001

Herrmann S, Kostrzewa M, Wierschem A, Streb C (2014) Polyoxometalate ionic liquids as self-repairing acid-resistant corrosion protection. Angew Chem Int Ed 53:13596–13599

Hu P et al (2014) Removal of organic pollutants from red water by magnetic-activated coke. Desalin Water Treat 54:2710–2722. doi:10.1080/19443994.2014.903204

Huang Y, Pan QY, Dong XW, Cheng ZX (2006) Synthesis and photochromism of a novel organic–inorganic hybrid film embedded with polyoxomatalates. Mater Chem Phys 97:431–436. doi:10.1016/j.matchemphys.2005.08.039

Hunger K (2007) Industrial dyes: chemistry, properties, applications. Wiley, Hoboken

Jensen JO (2002) Vibrational frequencies and structural determinations of hexamethylenetetraamine. Spectrochim Acta Pt A Mol Biomol Spectrosc 58:1347–1364

Jiang T, Y-d Liang, Y-j He, Wang Q (2015) Activated carbon/$NiFe_2O_4$ magnetic composite: a magnetic adsorbent for the adsorption of methyl orange. J Environ Chem Eng 3:1740–1751. doi:10.1016/j.jece.2015.06.020

Kan W-Q, Xu J-M, Kan Y-H, Guo J, Wen S-Z (2014) Syntheses, structures, and photocatalysis of five inorganic–organic hybrid compounds constructed from Keggin polyoxometalate clusters and multidentate N-donor ligands. J Coord Chem 67:195–214. doi:10.1080/00958972.2014.882503

Kida T, Furuso H, Kumamoto K, Pramata AD, Yuasa M, Shimanoe K (2015) Visible-light sensitization and photoenergy storage in quantum dot/polyoxometalate systems. Chem A Eur J 21:7462–7469

Kwiatkowski M, Chassagnon R, Heintz O, Geoffroy N, Skompska M, Bezverkhyy I (2017) Improvement of photocatalytic and photoelectrochemical activity of ZnO/TiO_2 core/shell system through additional calcination: insight into the mechanism. Appl Catal B Environ 204:200–208

Li F, Chen Y, Huang H, Cao W, Li T (2015) Removal of rhodamine B and Cr(VI) from aqueous solutions by a polyoxometalate adsorbent. Chem Eng Res Des 100:192–202. doi:10.1016/j.cherd.2015.05.030

Liu F, Chung S, Oh G, Seo TS (2012) Three-dimensional graphene oxide nanostructure for fast and efficient water-soluble dye removal. ACS Appl Mater Interfaces 4:922–927. doi:10.1021/am201590z

Liu X, Luo J, Zhu Y, Yang Y, Yang S (2015) Removal of methylene blue from aqueous solutions by an adsorbent based on metal-organic framework and polyoxometalate. J Alloys Compd 648:986–993. doi:10.1016/j.jallcom.2015.07.065

Liu X, Li Y, Peng S, Lai H, Yi Z (2016) Visible-light-driven hydrogen production in a dye sensitized polyoxometalate system without noble metals. Chem Phys Lett 651:238–242

Madrakian T, Afkhami A, Ahmadi M, Bagheri H (2011) Removal of some cationic dyes from aqueous solutions using magnetic-modified multi-walled carbon nanotubes. J Hazard Mater 196:109–114. doi:10.1016/j.jhazmat.2011.08.078

Madrakian T, Afkhami A, Mahmood-Kashani H, Ahmadi M (2012) Adsorption of some cationic and anionic dyes on magnetite nanoparticles-modified activated carbon from aqueous solutions: equilibrium and kinetics study. J Iran Chem Soc 10:481–489. doi:10.1007/s13738-012-0182-4

Muradov N, T-Raissi A (2006) Solar production of hydrogen using "self-assembled" polyoxometalate photocatalysts. J Sol Energy Eng 128:326–330

Omwoma S, Gore CT, Ji Y, Hu C, Song Y-F (2015) Environmentally benign polyoxometalate materials. Coord Chem Rev 286:17–29. doi:10.1016/j.ccr.2014.11.013

Ou S, Zheng J-P, Kong G-Q, Wu C-D (2015) Designed synthesis of a series of zwitterion–polyoxometalate hybrid materials for selective scavenging and photolysis of dyes. Dalton Trans 44:7862–7869

Pang H, Niu Y, Yu J, Ma H, Song Q, Li S (2015) Synthesis, structure, and photocatalytic property of a new hybrid compound based on unusual bi-silver-capped polyoxometalates. Inorg Chem Commun 59:5–8

Pu Y-C, Chou H-Y, Kuo W-S, Wei K-H, Hsu Y-J (2017) Interfacial charge carrier dynamics of cuprous oxide-reduced graphene oxide (Cu_2O-rGO) nanoheterostructures and their related visible-light-driven photocatalysis. Appl Catal B Environ 204:21–32

Rajabi HR, Arjmand H, Hoseini SJ, Nasrabadi H (2015) Surface modified magnetic nanoparticles as efficient and green sorbents: synthesis, characterization, and application for the removal of anionic dye. J Magn Magn Mater 394:7–13. doi:10.1016/j.jmmm.2015.06.024

Singh G, Baranwal BP, Kapoor IPS, Kumar D, Fröhlich R (2007) Preparation, X-ray crystallography, and thermal decomposition of some transition metal perchlorate complexes of hexamethylenetetramine. J Phys Chem A 111:12972–12976. doi:10.1021/jp077278z

Song S, Ma Y, Shen H, Zhang M, Zhang Z (2015) Removal and recycling of ppm levels of methylene blue from an aqueous solution with graphene oxide. RSC Adv 5:27922–27932. doi:10.1039/c4ra16982d

Streb C (2012) New trends in polyoxometalate photoredox chemistry: from photosensitisation to water oxidation catalysis. Dalton Trans 41:1651–1659. doi:10.1039/c1dt11220a

Taghdiri M, Zamani N (2013) Hexamine adsorption study on activated carbon from aqueous solutions for application in treatment of hexamine industrial wastewater. Int J Environ Sci Technol 10:19–26

Taghdiri M, Saadatjou N, Zamani N, Farrokhi R (2013) Heterogeneous degradation of precipitated hexamine from wastewater by catalytic function of silicotungstic acid in the presence of H_2O_2 and H_2O_2/Fe^{2+}. J Hazard Mater 246:206–212

Taghdiri M, Zamani N, Mousavian SA (2015) Study of hexamine removal by activated carbon modified with magnetic iron oxide nanoparticles for application in treatment of hexamine industrial wastewater. Desalin Water Treat 56:3323–3333

Troupis A, Triantis T, Gkika E, Hiskia A, Papaconstantinou E (2009) Photocatalytic reductive–oxidative degradation of Acid Orange 7 by polyoxometalates. Appl Catal B Environ 86:98–107

Trzesowska A, Kruszynski R (2008) Channel-containing structure built of 3D sodium nitrate coordination polymer. J Coord Chem 61:2167–2177

Wang W, Yang S (2010) Photocatalytic degradation of organic dye methyl orange with phosphotungstic acid. J Water Res Prot 2:979

Wang X-L, Gong C-H, Zhang J-W, Liu G-C, Kan X-M, Xu N (2015a) Polyoxometalate-directed assembly of various multinuclear metal–organic complexes with 4-amino-1,2,4-triazole and selective photocatalysis for organic dye degradation. CrystEngComm 17:4179–4189

Wang X, Chang Z, Lin H, Tian A, Liu G, Zhang J, Liu D (2015b) Effect of polyoxoanions and amide group coordination modes on the assembly of polyoxometalate-based metal–organic complexes constructed from a semi-rigid bis-pyridyl-bis-amide ligand. CrystEngComm 17:895–903

Wang X-L, Zhang R, Wang X, Lin H-Y, Liu G-C (2016) An effective strategy to construct novel polyoxometalate-based hybrids by deliberately controlling organic ligand transformation in situ. Inorg Chem 55:6384–6393

Yang N, Zhu S, Zhang D, Xu S (2008) Synthesis and properties of magnetic Fe_3O_4-activated carbon nanocomposite particles for dye removal. Mater Lett 62:645–647. doi:10.1016/j.matlet.2007.06.049

Yang S-T, Chen S, Chang Y, Cao A, Liu Y, Wang H (2011) Removal of methylene blue from aqueous solution by graphene oxide. J Colloid Interface Sci 359:24–29. doi:10.1016/j.jcis.2011.02.064

Ye T, Wang J, Dong G, Jiang Y, Feng C, Yang Y (2016) Recent progress in the application of polyoxometalates for dye-sensitized/organic solar cells. Chin J Chem 34:747–756

Yin M, Li Z, Kou J, Zou Z (2009) Mechanism investigation of visible light-induced degradation in a heterogeneous TiO2/Eosin Y/Rhodamine B system. Environ Sci Technol 43:8361–8366

Zargar B, Parham H, Hatamie A (2009) Fast removal and recovery of amaranth by modified iron oxide magnetic nanoparticles. Chemosphere 76:554–557. doi:10.1016/j.chemosphere.2009.02.065

Zargar B, Parham H, Rezazade M (2011) Fast removal and recovery of methylene blue by activated carbon modified with magnetic iron oxide nanoparticles. J Chin Chem Soc 58:694–699

Zhai Q, Zhang L, Zhao X, Chen H, Yin D, Li J (2016) A novel iron-containing polyoxometalate heterogeneous photocatalyst for efficient 4-chlorophennol degradation by H_2O_2 at neutral pH. Appl Surf Sci 377:17–22. doi:10.1016/j.apsusc.2016.03.083

Zhang Z, Kong J (2011) Novel magnetic Fe_3O_4@C nanoparticles as adsorbents for removal of organic dyes from aqueous solution. J Hazard Mater 193:325–329. doi:10.1016/j.jhazmat.2011.07.033

Zhang L, Chen H, Zhao X, Zhai Q, Yin D, Sun Y, Li J (2016) The marriage of ferrocene and silicotungstate: an ingenious heterogeneous Fenton-like synergistic photocatalyst. Appl Catal B Environ 193:47–57

Zhou E-L, Qin C, Wang X, Shao K-Z, Su Z-M (2016) Assembly of two novel 3D organic-inorganic hybrids based on Keggin-type polyoxometalates: syntheses, crystal structures and properties. CrystEngComm. doi:10.1039/c6ce00021e